https://doi.org/10.1016/j.energy.2021.121766

Deciphering the Optimal Exergy Field In Closed-wet Cooling Towers Using Bi-level Reduced-order Models

Jinghui Qu[1], Mingjian Li[1], Chang He[2*], BingJian Zhang[2], QingLin Chen[2], Jingzheng Ren[3]

[1]School of Chemical Engineering and Technology, Sun Yat-Sen University, Zhuhai, China

[2]School of Materials Science and Engineering, Guangdong Engineering Centre for Petrochemical Energy Conservation, Sun Yat-sen University, Guangzhou, 510275, China.

[3]Department of Industrial and Systems Engineering, The Hong Kong Polytechnic University, Hong Kong Special Administrative Region, China

E-mail: hechang6@mail.sysu.edu.cn

Submit to Special Issue of *Energy* dedicated to PRES'20

Abstract: This paper introduces a bi-level reduced-order models (ROMs) approach for quickly deciphering the optimal exergy fields in closed wet cooling towers (CWCTs) with consideration of weather variations. First, an efficient sampling method based on stochastic reduced-order model is performed for the approximation of the multivariate probability distributions by generating a finite set of samples. The uncertainty associated with input variables is propagated via multi-sample CFD simulations of the CWCT model for each of the samples. The results of the state and output variables stored in the CFD solutions are used to construct the data-driven and physics-based ROMs by combining principal component analysis and artificial neural network methods. The constructed data-driven ROM is embedded in a sampling-based stochastic optimization model that seeks the maximization of the expected exergy efficiency ratio. The physics-based ROM is used to visualize the optimal field profiles of the thermal-, mechanical-, and chemical- exergy fluxes. Finally, the results of a case study demonstrate that the main strengths of the proposed approach is to simultaneously obtain the optimal exergy efficiency ratios and the exergy field profiles of the CWCT system in a computationally efficient manner.

Keywords: Reduced-order models, Closed wet cooling towers, Exergy fields, Exergy efficiency ratio, Stochastic optimization, Stochastic reduced-order model

Nomenclature

A	heat and mass transfer area (m^2)	Greek Symbols	
B	mapping coefficient	α	reduced rank
C	heat capacity (J/kg·°C)	σ	singular value
D	mapping coefficient	δ	weighting factor
E	expected value	$\boldsymbol{\varepsilon}$	remaining noise
F	mapping function	λ	eigenvalue
G	mapping function	μ	moment
$\mathbf{I}$	unit matrix	φ	relative humidity (%)
J	exergy flux (W/m^2)	γ	number of elements
L	number of layers	ω	humidity ratio (kg/kg)
M	eigenvectors	η	mechanical efficiency
N	number of samples	$\mathbf{\Sigma}$	diagonal matrix
P	pressure (Pa)	Ψ	principal component matrix
Q	energy consumption (W)	Φ	score matrix
R	gas constant (J/kg·°C)		
T	temperature (°C)	Subscripts	
V	eigenvectors	a	air
$\boldsymbol{X}$	input space	v	vapour
$\boldsymbol{Y}$	output space	0	dead state
$\boldsymbol{Z}$	state space	$them$	thermal exergy
a	outputs from neuron	$mech$	mechanical exergy
$\mathbf{b}$	weighting parameter	$chem$	chemical exergy
e	deviation	cw	circulating water
g	gravity acceleration (m/s^2)	sw	spray water
h	differential head (m)	sp	spray pump
l	number of neurons	fan	fan blade
m	number of outputs	$belt$	belt
$\dot{m}$	flow rate	$motor$	motor
n	number of inputs	TE	test set
q	q-order moments		
$\boldsymbol{r}$	correlation matrix	Superscripts	
s	number of state variables	in	input conditions
$\boldsymbol{x}$	input vectors	out	output conditions
$\boldsymbol{y}$	output vectors		
$\boldsymbol{z}$	state vectors		
ex	exergy (J/kg)		
Ex	exergy flow(W)		
Pr	probability function		
$prob$	sample probability		
EER	exergy efficiency ratio		
IW	weighting parameter		
LW	weighting parameter		

1 Introduction

Incorporation of the emerging closed wet cooling towers (CWCTs) in the cooling water system has been regarded as a viable path to reduce water consumption in thermal systems [1]. In CWCTs, coupled heat and mass transfer processes between humid air and water are the most common and fundamental phenomenon [2]. Exergy analysis is an effective theoretical tool for investigating the thermodynamic irreversibility of such processes. It exploits both the qualitative and quantitative natures of energy, and thus represents the true potential of a cooling tower to perform optimal work relative to a dead state [3]. The past studies mainly applied it to investigate entropy generation [4], exergy destruction [5], process efficiency [6], and system optimization [7] of cooling towers. These studies based on traditional exergy analysis and system-level flowsheets only consider the lumped parameters description of input-output streams with many ideal assumptions. There are rarely studies on the description of the spatially distributed parameters inside of the cooling tower systems despite its importance.

The distributed first-principle models provide an accurate physical description of the coupled heat and mass transfer processes by considering the detailed multiphase interactions, transport effects, and phenomena at a broader length scale. It is significant for equipment design and flow field analysis due to the benefits of energy-saving, cost reduction, and process intensification. For example, the state profiles of temperature and humidity of the inlet air in the air-liquid contact units of the cooling towers are unevenly distributed and varied with uncertain and control parameters, which define the spatial heterogeneities of the humid and thermal exergies of the air in the flow field.

The distributed exergy parameters contain the microscopic information of the transport effects in the state space. Deciphering such exergy field profiles in detail is conducive to improve the overall thermodynamic performance of the cooling towers due to the obtained understanding of the infinitesimal heat and mass transfer processes.

In theory, the spatially distributed exergy analysis can be realized through multi-phase field numerical simulation of the full-order model (FOM) with the advance of distributed parameter computational fluid dynamics (CFD). Nevertheless, the solution of the CWCT's FOM involves tracking the multiphase interactions and the spatial movement of each liquid droplet characterized by computationally expensive partial differential equations (PDEs). For instance, a single task of the 3-D CFD model of CWCT normally takes more than 30 CPU hours by using Reynolds averaged Navier-Stokes equations [8]. The computational burden would significantly limit the use of the principled CFD simulation for real-time prediction and multivariable analysis. It becomes more critical as the FOM is encountered in an equation-oriented optimization task because a large size of recourses to the CFD models have to be executed before converging to the optimum. Therefore, the benefits of spatially distributed exergy analysis must be weighed against the time necessary to obtain them, which is a major cost driver and impedes developing processes with optimal flow field of exergy.

The reduced-order model (ROM) of a CFD-based model is a surrogate model for input-to-output mapping due to the computationally expensive nature of high-fidelity simulation which entails iterative calculations [9]. Surrogate-based model reduction is one of the practical solutions to construct a more tractable model as an alternative for

computationally expensive FOMs without loss of fidelity by only approximating the input-output relation of a system [10]. Given input parameters (i.e., initial, boundary, and operational conditions), the quantities of interest for calculating exergy flow at each mesh point, such as velocity, pressure, temperature, and moisture content can be obtained rapidly without conducting principled CFD simulation.

The model reduction approach can be roughly categorized into two: physics-based models and data-driven models [11]. In the former, a reduced basis is extracted from the simulation data using an unsupervised learning technique, e.g., principal component analysis (PCA) [12], by which the FOM operator is projected onto the subspace spanned by the reduced basis [13]. As a result, the degrees of freedom of the original system can be significantly reduced by retaining the underlying basic structure of the FOM. Another way to enable rapid simulations is to build a data-driven model, where a response surface of the system is learned from the simulation data in a supervised manner. The deterministic or probabilistic mapping models of input-output can be constructed using statistical methods, e.g., polynomial basis functions [14], radial basis functions [15], Gaussian process [16], and stochastic polynomial chaos expansion [17], etc. All these models are built upon the CFD solutions of design points in parameter space.

Besides, existing studies typically assume that the weather conditions are perfectly known or even fixed in advance without considering seasonal variability, leading to an over-optimistic design or underestimation of the thermodynamic performances of the cooling towers. In practice, the operation of a cooling tower is closely related to the

fluctuating weather conditions, and multiple types of uncertainties (i.e., temperature and humidity) strongly affect the characteristics of heat and mass transfer processes, especially in extreme conditions. There may be abnormal operations in which the tasks of the cooling tower systems cannot be fulfilled due to the relatively small evaporation. Thus, there is a need to develop rapid and accurate predictive models that help designers and researchers to investigate the thermodynamic performances of the cooling towers under uncertain weather conditions.

This work aims to address the aforementioned issues through the development of a bi-level ROMs approach that comprises data-driven ROM and physics-based ROM for obtaining the optimal exergy fields in CWCTs with consideration of weather variations. The remainder of the paper is organized as follows. Section 2 introduces the derivation of the model objective including exergy efficiency ratio and exergy flows. Section 3 contains a detailed description of the model reduction techniques, i.e., design of optimal experiment, multi-sample CFD simulation, bi-level ROMs construction, and model evaluation. Section 4 briefly describes the stochastic optimization model. The application of this approach is shown through a case study of a small size CWCT system in the following section. Finally, it concludes with a discussion and future perspectives in Section 6.

2 Exergy efficiency ratio and exergy flux

In a cooling tower system, the exergy of humid air represents the maximum useful work done by inlet air as it is gradually saturated and approaches an equilibrium state relative to the dead state. In general, it can be broken down into thermal, mechanical,

and chemical ones, as defined by Eqs. (1~3), respectively.

$$ex_{a,them}(\mathrm{T},\omega)=(\mathrm{C}_a+\omega_a C_v)\times(\mathrm{T}_a-\mathrm{T}_0-T_0\ln\frac{T_a}{T_0}) \tag{1}$$

$$ex_{a,mech}(T,\omega)=RT_0(1+1.608\omega_a)\ln\frac{P_a}{P_0} \tag{2}$$

$$ex_{a,chem}(\omega)=RT_0\{(1+1.608\omega_a)\ln\frac{1+1.608\omega_0}{1+1.608\omega_a}+1.608\omega_a\ln\frac{\omega_a}{\omega_0}\} \tag{3}$$

where C and R are the specific heat capacity and gas constant; T, P, and ω are the dry-bulb temperature, pressure, and humidity; the subscripts *0*, *a*, and *v* are the dead state, air, and vapour, respectively. Note that, the reference condition at ambient temperature with saturated humidity ratio is selected as the dead state [18].

Multiplying the exergy by the mass flow rate gives the exergy flow of humid air:

$$\dot{E}x_{a,i}^{j}(T,\omega,\dot{m})=ex_{a,i}^{j}\times\dot{m}_a,\quad i=\{them,mech,chem\}\quad j=\{in,out\} \tag{4}$$

The inlet circulating water is cooled down by the water film outside the tubes as it passes through the coil section in a steady state. Here, the chemical exergy is ignored and thus the exergy flow is the sum of thermal and mechanical ones, as given in Eq. (5). Meanwhile, the circulations of air and spray water streams entering the CWCT system are sustained by the intake fan and spray pump. The total exergy of electricity consumed by the auxiliary equipment can be calculated via Eq. (6).

$$\dot{E}x_{cw}^{j}(\dot{m},T)\approx\dot{m}_{cw}C_{\mathrm{c}w}(T_{cw}^{j}-T_0-T_0\ln\frac{T_{cw}^{j}}{T_0})+\dot{m}_{cw}(\frac{P_{cw}^{j}}{P_0}),\quad j=\{in,out\} \tag{5}$$

$$\dot{E}x_{aux}(\dot{m})=Q_{sp}+Q_{fan}=\dot{m}_{sw}gh/\eta_{sp}+\dot{m}_a\Delta P/(\rho_a\eta_{fan}\eta_{belt}\eta_{motor}) \tag{6}$$

where g, h, Q, and η are the gravitational acceleration, differential head, energy consumption, and mechanical efficiency, respectively; the subscripts *sp*, *cw*, *sw, fan*,

belt, and *motor* are the spray pump, circulating water, spray water, fan blade, belt, and motor, respectively.

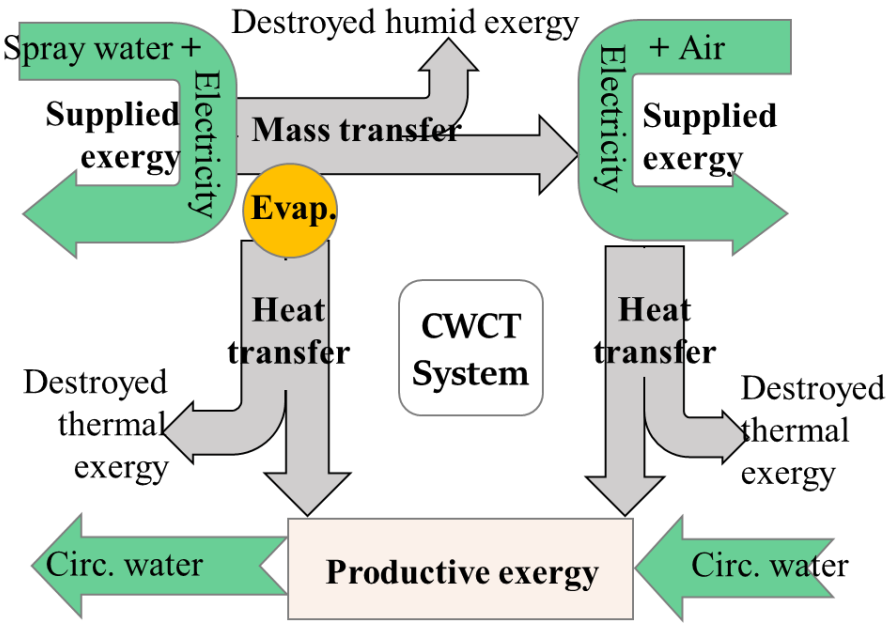

Fig. 1. Schematic diagram of exergy flows in a CWCT system.

Fig. 1 illustrates the input and output of exergy flows of the investigated CWCT system. The fundamental goal of this system is to cool down the input circulating water by exchanging sensible heat with liquid film and air flow outside the tubes. To achieve this goal, the supplied exergies of all participating streams (spray water and air, etc.) and electrical energy (intake fans, pumps, etc.) should be effectively transformed into the productive thermal exergy of circulating water while minimizing the destroyed thermal and humid exergies. Herein, the exergy efficiency ratio (EER) defined in Eq. 7 is employed to reveal the degree of effective use of available supplied exergies which are required to maintain the heat and mass transfer processes in a CWCT system.

$$EER = \frac{\text{productive exergy}}{\text{supplied exergy}} = \frac{\dot{E}x_{cw}^{in} - \dot{E}x_{cw}^{out}}{\dot{E}x_{a}^{in} + \dot{E}x_{cw}^{in} + \dot{E}x_{aux}} \tag{7}$$

where *Ex* is the exergy flow rate; the superscripts *in* and *out* are the input and output

streams, respectively.

In this study, a new state variable is introduced, namely exergy flux (W/m^2, similar to heat flux) for exploring the density of exergy flow of the humid air in the fluid field. The exergy flux includes the thermal, mechanical, and chemical components, which can be regarded as different types of distributed exergy flows per unit of area (dA). As defined in Eq. (8), it is a product of the exergy and the mass flux (j_a).

$$\vec{J}_{a,i} = \dot{E}x_{a,i}/dA = ex_{a,i}\, j_a, \quad i = \{therm, mech, chem\} \tag{8}$$

3 Development of the bi-level ROMs

Given an equipment item, the model reduction involves three types of variable spaces: input space **X**, output space **Y**, and state-space **Z** in the fluid field. Fig. 2 shows the interconnection of the matrices of these three variable spaces for constructing the bi-level ROMs. As shown, the CWCT system has n inputs and m outputs while s state variables are monitored in a total of γ discretized elements. The nonlinear relationships of the state and output variables corresponding to its input variables can be expressed by the following state-space model in steady state [19]:

$$\begin{bmatrix} \boldsymbol{y} \\ \boldsymbol{z} \end{bmatrix} = \begin{bmatrix} \mathbf{B}(\boldsymbol{x}) \\ \mathbf{D}(\boldsymbol{x}) \end{bmatrix} \tag{9}$$

where $\boldsymbol{B}$ and $\boldsymbol{D}$ are the mapping coefficient matrices; $\boldsymbol{x}$, $\boldsymbol{y}$, and $\boldsymbol{z}$ are the input, output, and state vectors, respectively, which contain the variables related to calculate exergy efficiency ratio and exergy flow field.

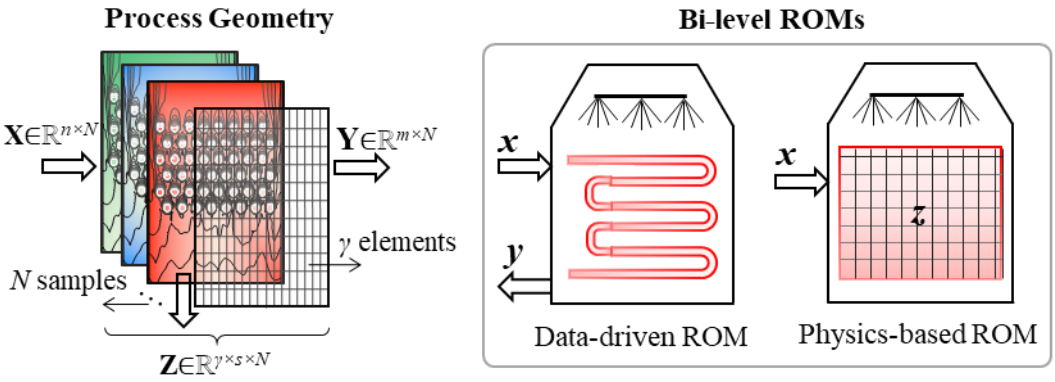

Fig. 2. Interconnection of the variable spaces used in the construction of bi-level ROMs of CWCTs.

The input, output, and state spaces for the CFD model of CWCTs should be defined before the experimental design. The input vector $\boldsymbol{x}$ in the input space is provided in Table 1. For a given inlet boundary condition, it contains the values of all variables in the input streams entering the cooling tower system, i.e., control variable $\boldsymbol{x}^{(2)}=[\dot{m}_a, \dot{m}_{sw}]^{\mathrm{T}}$ and uncertain variable $\boldsymbol{x}^{(1)}=[T_a^{in}, \varphi_a^{in}]^{\mathrm{T}}$. Similarly, the output vector $\boldsymbol{y}$ in the output space contains the values of all variables in the output streams, $\boldsymbol{y}=[T_{cw}^{out}, T_a^{out}, \varphi_a^{out}]^{\mathrm{T}}$. Note that, the exergy efficiency ratio calculation requires the results of both the input vector $\boldsymbol{x}$ and the corresponding output vector $\boldsymbol{y}$. The state space is spatially distributed and bounded by the equipment geometry. The state vector $\boldsymbol{z}$ in the state space accommodates the values of exergy fluxes at each discretized node of the mesh, $\boldsymbol{z}=[J_{a,therm}, J_{a,mech}, J_{a,chem}]^{\mathrm{T}}$.

For constructing the bi-level ROMs of CWCTs with high fidelity, it is necessary to build the mappings between the aforementioned input and output vectors, as well as between the input and state vectors. For this purpose, much effort is required to collect and handle a huge amount of data obtained from a batch of principled CFD simulations

of the equipment item. The main steps are summarized as follows

STEP 1: Implement a DoE in the specific ranges to obtain a finite set of samples over the input domain.

STEP 2: Solve the CFD cases one by one with the obtained samples under the defined mesh system. The results of the state and output variables of interest are retrieved from the information stored in the CFD solutions.

STEP 3.1: Implement the mapping $\boldsymbol{x}\rightarrow\boldsymbol{y}$ and then formulate the data-driven ROM.

3.2: PCA is performed for the dimension reduction of obtained z to obtain the ranked principal components, loadings matrix, and score matrix $\boldsymbol{\Phi}$, and then implement the mapping $\boldsymbol{x}\rightarrow\boldsymbol{\Phi}$ and formulate the physics-based ROM.

STEP 4: Evaluate the generalization performance of the developed bi-level ROMs.

More details about these four steps are provided in the following sections 3.1~3.4.

Table 1. Input space for the model parameters

Input domain	Symbol	Unit	Specification
Control variable $\mathbf{X}^{(1)}$			
volume flow rate of air	$\dot{m}_a$	m^3/s	U[1.0, 3.0]
mass flow rate of spray	$\dot{m}_{sw}$	kg/s	U[1.0, 2.0]
Uncertain variable $\mathbf{X}^{(2)}$			
dry bulb temp. of air	T_a	°C	uncertain variable
relative humidity of air	φ_a	-	uncertain variable

3.1 Design of optimal experiments

The batch simulation of the principled CFD model is often computationally costly and time-consuming, which entails the need to reduce computational resources. DoE is

a well-suited approach as it is capable of maximizing the amount of process information obtained from a fixed size of observations through properly selecting design points. There are various methods available for implementing a DoE, i.e., Monte-Carlo sampling, Taguchi experiment, probabilistic collocation, stochastic collocation, etc. Herein, a low dimensional, discrete approximation method, namely stochastic reduced-order model (SROM)[20], is used to generate a finite size of stochastic samples with varying probability. The SROM method can be viewed as a "smart" Monte Carlo method for uncertainty quantification [21], which can efficiently discretize the input space and significantly reduce the model complexity associated with propagated uncertainty while retaining the benefit of being a non-intrusive method. The detailed description of this method is as follows.

Let us consider the probabilistic behavior of $\mathbf{X}=\{\mathbf{x}_i\}_{i=1}^{n}$ to be specified with known expressions for its marginal distributions, moments of order q, and correlation matrix as:

$$\mathrm{F_i}(\theta)=\Pr\left(\mathbf{x}_i\le\theta\right),\quad i=1,\ldots,n \tag{10}$$

$$\mu_i(q)=\mathrm{E}\left[\mathbf{x}_i^q\right],\quad i=1,\ldots,n \tag{11}$$

$$\mathbf{r}=\mathrm{E}\left[\mathbf{X}\mathbf{X}^{\mathrm{T}}\right] \tag{12}$$

An SROM $\tilde{\mathbf{X}}\in\mathbb{R}^{n\times N}$ is an approximation of the $\mathbf{X}$ in the sense that $\tilde{\mathbf{X}}$ and $\mathbf{X}$ have similar statistical properties. The SROM $\tilde{\mathbf{X}}$ consists of a sample set $\left\{\tilde{\mathbf{x}}^{(j)}\right\}_{j=1}^{N}$ with the corresponding probabilities $\left\{prob^{(j)}\right\}_{j=1}^{N}$, thus $\sum_{j=1}^{N}prob^{(j)}=1$. Each sample $\tilde{\mathbf{x}}^{(j)}=\left\{\tilde{x}_i^{(j)}\right\}_{i=1}^{n}$ contains one or multiple values depending on the dimension of $\mathbf{X}$.

Similar to $\mathbf{X}$, the statistics of the SROM $\tilde{\mathbf{X}}$ are as follows

$$\tilde{\mathrm{F}}_i(\theta)=\sum_{j=1}^{N} prob^{(j)}\,\mathrm{I}\left(\tilde{x}_i^{(j)}\le\theta\right)\quad i=1,\ldots,n \tag{13}$$

$$\tilde{\mu}_i(q)=\sum_{j=1}^{N} prob^{(j)}\left(\tilde{x}_i^{(j)}\right)^q\quad i=1,\ldots,n \tag{14}$$

$$\tilde{r}(i_1,i_2)=\sum_{j=1}^{N} prob^{(j)}\tilde{x}_{i_1}^{(j)}\tilde{x}_{i_2}^{(j)}\quad i_1,i_2=1,\ldots,n \tag{15}$$

where I(A) is a binary function, I(A)=1 if A is true, otherwise I(A)=0. The discrepancy between $\tilde{\mathbf{X}}$ and $\mathbf{X}$ in the statistical sense is represented by the distribution deviation e_1, the moment deviation e_2, and the correlation matrix deviation e_3:

$$e_1(\mathbf{X},\boldsymbol{prob})=\frac{1}{2}\sum_{i=1}^{n}\sum_{j=1}^{N}\left[\tilde{\mathrm{F}}_i\left(\tilde{x}_i^{(j)}\right)-\mathrm{F}_i\left(\tilde{x}_i^{(j)}\right)\right]^2 \tag{16}$$

$$e_2(\mathbf{X},\boldsymbol{prob})=\frac{1}{2}\sum_{i=1}^{n}\sum_{q=1}^{\bar{q}}\left(\frac{\tilde{\mu}_i(q)-\mu_i(q)}{\mu_i(q)}\right)^2 \tag{17}$$

$$e_3(\mathbf{X},\boldsymbol{prob})=\frac{1}{2}\sum_{i_1,i_2=1;i_2>i_1}^{n}\left(\frac{\tilde{r}(i_1,i_2)-r(i_1,i_2)}{r(i_1,i_2)}\right)^2 \tag{18}$$

The optimal SROM $\tilde{\mathbf{X}}$ for $\mathbf{X}$ with the minimum deviation can be obtained using the following optimization algorithm:

$$\begin{aligned}\mathbf{X}\equiv\underset{\tilde{\mathbf{x}},\,\boldsymbol{prob}}{\arg\min}&\left(\sum_{i=1}^{3}\delta_i e_i(\mathbf{X},\boldsymbol{prob})\right)\\ s.t.\quad&\sum_{j=1}^{N} prob^{(j)}=1\\ &prob^{(j)}\ge 0,\quad j=1,\ldots,N\end{aligned} \tag{19}$$

where the coefficients $\{\delta_i\ge 0\}_{i=1}^{3}$ are the weighting factors to control the contribution of each error term to the objective function. The determination of sample size N is dependent on computational considerations, and the optimal solution can be considered as a good approximation of the original distribution. [22]

3.2 Multi-sample CFD simulations

To obtain the mapping data for constructing the ROMs, the uncertainty associated with the input variables are propagated by executing the rigorous CFD simulation of the CWCT model for each of the SROM samples. Fig. 3(a) shows the sketch of the experimental prototype of the CWCT system under investigation. The core of this system is the staggered tube bundle at the coil section, which provides the main areas for heat and mass transfer processes between counter-current spray water and air. A small proportion of spray water diffuses to the upward airflow due to evaporation, while the remaining portion leaving the liquid film is collected in a water tank and finally returns to the top nozzles via spray pump. The circulating water inside of the tubes relies on film evaporation to achieve the required cooling target, such as temperature drop and heat dissipation. Thus, this study only focuses on the heat and mass transfer processes of the water film outside the tube bundle at the coil section, which is stimulated by a 3-D CFD model of flow, temperature, and pressure fields.

The process geometry of the coil section shown in Fig. 3(b) is constructed based on the standard diameter and length in the COMSOL modeling environment. The cross-section of the tube bundle is in a triangular arrangement, and the arbitrary adjacent tubes in each row have the same centerline spacing, as shown in Fig. 3(c). It consists of 19 rows and 12 columns of bare-type copper tubes in the 0.61×1.2×0.68 m domain. The preliminary sketch is meshed to adequately capture the change of fluids by using the Meshing Module. To improve the accuracy and stability, a five-layer boundary layer grids with stretching factor 1.2 is adopted for both inside and outside of the tube walls, while the remaining space is filled using free tetrahedral meshes. Note that, the meshes

near the tube walls are refined to improve the model accuracy, while the element size is smoothly stretched to ensure an accurate resolution of the high gradient regions of the fluid fields. Besides, only half of the adjacent tubes have been investigated due to the geometric symmetry. Thus, the computational domain is extended by 0.09m, 1.2 m, 0.68 m in x, y, and z axes, respectively. The mesh structure has 1,114,893 nodes, and only 3,304 nodes are presented in the cross-section along the center of the coil tube. The quality of this mesh structure measured by the skewness value should be satisfied with the required level.

The multi-sample CFD simulation is performed on the meshed geometry of the CWCT system to calculate the coupled heat and mass transfer processes, as well as the mass and energy balances of the PDEs. In each CFD model, the RNG k-ε turbulence modelling approach is applied to simulate the mean flow characteristics of the air and water in turbulent flow conditions. The governing equations with boundaries are solved by the finite element method, and a segregated solver sequence was selected to handle the highly non-linear models. Moreover, the source terms of the moisture transport and heat transfer are added to the governing equations for accurately describing the heat and mass transfer processes. The detailed descriptions of the governing equations, source terms, and boundary conditions are provided in Supplementary Information-1 (SI-1).

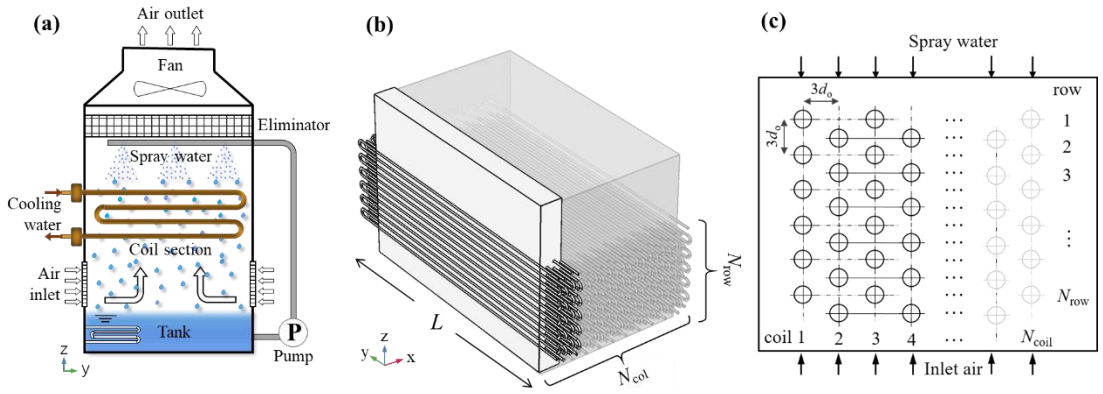

Fig. 3. The schematics of (a) the CWCT set-up, the (b) coil section, and the (c) cross-section of the tube bundle.

3.3 Model reduction

In this step, the results of the state and output variables stored in the CFD solutions are used to construct the physics-based and data-driven ROMs by combining PCA and ANN approaches. The data-driven ROM of CWCTs expressed as a set of equations is formulated by implementing the mapping from the input vector to the output vector, $\boldsymbol{x}\rightarrow\boldsymbol{y}=\mathbf{G}(\boldsymbol{x})$. This mapping is important for integration of the equipment model within the simulator for simulation and optimization, which can be built by using a surrogate-based prediction method such as artificial neural network (ANN), partial least squares, Kriging, etc. In this study, an L-layer ANN with n inputs, l neurons in the hidden layer, and m targets in the output layer is applied to implement this mapping. Herein, the input of the ANN, $\mathbf{X}=[\boldsymbol{x}^{(1)}, \boldsymbol{x}^{(2)}]\in\mathbb{R}^{n\times N}$, contains the all control and uncertain variables (see Table 1) stored a set of N CFD simulations, while the output refers to the all variables in the output streams, $\boldsymbol{y}=[T_{cw}^{out}, T_a^{out}, \varphi_a^{out}]^{\mathrm{T}}$. Besides, a hyperbolic tangent sigmoid function $f(\cdot)=\mathrm{tansig}(x)$ is used as the active function of the hidden layer because of its preferable nonlinearity and continuity property of the first-order derivative. In all, the

ANN model is as follows:

$$x_i' = \frac{2\left(x_i - x_{\min,i}\right)}{\left(x_{\max,i} - x_{\min,i}\right)} - 1 \quad i = 1,...,n \tag{20-1}$$

$$a_j' = \sum_{i=1}^{n} IW_{j,i} x_i' + b_{1,\mathrm{j}} \quad j = 1,...,l \tag{20-2}$$

$$a_j = f(a_j') = \frac{2}{\left(1 + e^{-2a_j'}\right)} - 1 \quad j = 1,...,l \tag{20-3}$$

$$y_k' = \sum_{j=1}^{l} LW_{j,k} x_j' + b_{2,k} \quad k = 1,...,m \tag{20-4}$$

$$y_k = \frac{1}{2}\left(y_k' + 1\right)\left(y_{\max,k} - y_{\min,k}\right) + y_{\min,\mathrm{k}} \quad k = 1,...,m \tag{20-5}$$

where x', a' and y' are the scaled inputs, intermediate outputs from neurons, and scaled outputs, respectively.

This neural network mapping is trained with Bayesian regularization to obtain the following weighting parameters: $\mathbf{IW} \in \mathbb{R}^{l \times n}$, $\mathbf{LW} \in \mathbb{R}^{l \times m}$, $\mathbf{b_1} \in \mathbb{R}^{l}$, $\mathbf{b_2} \in \mathbb{R}^{m}$. Therefore, the neural network mapping is expressed by purely linear correlations in a matrix form:

$$\boldsymbol{y} = \mathrm{G}(\boldsymbol{x}) = \mathrm{LW}^{\mathrm{T}}\left[f\left(\mathrm{IW} \cdot \boldsymbol{x} + \boldsymbol{b}_1\right)\right] + \boldsymbol{b}_2 \tag{21}$$

The physics-based ROM of CWCTs is constructed by implementing the input-to-state mappings through a snapshot PCA-ANN approach. As shown in Fig. 4, the PCA decomposition is first used to reduce the dimension of the state space**.** It can construct a reduced number of orthonormal basis vectors in a subspace that expresses a random vector of higher dimensionality without significant loss of data information. In particular, a specific state-space snapshot matrix $\mathbf{Z}_i \in \mathbb{R}^{\gamma \times N}$ can be decomposed after eliminating zeros as

$$\mathbf{Z}_i = \mathbf{M\Sigma V}^T \quad i = 1,\ldots,s \tag{22}$$

where the diagonal matrix $\mathbf{\Sigma}$=diag(σ_1, σ_2,…, σ_N) contains singular values of matrix $\mathbf{Z}_i$ in descending order, and square matrix $\mathbf{M} \in \mathbb{R}^{\gamma \times \gamma}$ and $\mathbf{V} \in \mathbb{R}^{N \times N}$ are the eigenvectors of $\mathbf{Z}_i\mathbf{Z}_i^{\mathbf{T}}$ and $\mathbf{Z}_i^{\mathbf{T}}\mathbf{Z}_i$ with the corresponding eigenvalues $\lambda_j=\sigma_j^2$, respectively.

The singular values of each variable in each eigenvector signifies the importance of this variable to the new vector space. Note that, σ declines rapidly with the rank order of $\sigma_1 \geq \sigma_2 \ldots \geq \sigma_N$, in most cases the sum of the top 10% of σ can account for more than 95% of the total singular values. Reducing to rank α resulting from the cutoff criterion, the α-order reduced data set is expressed as

$$\mathbf{Z}_i \approx \mathbf{Z}_i^{(\alpha)} = \mathbf{M}^{(\alpha)}\mathbf{\Sigma}^{(\alpha)}\left(\mathbf{V}^{(\alpha)}\right)^{\mathbf{T}} \tag{23}$$

where the superscript (α) that indicates the first α columns are taken from the original matrix to formulate a new matrix ($\alpha << \gamma$). Then, the matrix $\mathbf{Z}_i$ can be expressed as:

$$\mathbf{Z}_i = \mathbf{\Psi\Phi} + \boldsymbol{\varepsilon} \tag{24}$$

where matrix $\mathbf{\Psi}=\mathbf{M}^{(\alpha)} \in \mathbb{R}^{\gamma \times \alpha}$ is the principal component (PC) matrix; $\mathbf{\Phi}=\mathbf{\Sigma}^{(\alpha)}(\mathbf{V}^{(\alpha)})^{\mathbf{T}} \in \mathbb{R}^{\alpha \times N}$ is the score matrix of the transformed elements in the new vector space; $\boldsymbol{\varepsilon}$ is the remaining noise.

The dominant variances in the PC space that are captured by the α-order reduced data set can be determined from

$$R_\alpha = \sum_{j=1}^{\alpha}\lambda_j / \sum_{j=1}^{N}\lambda_j = \sum_{j=1}^{\alpha}\sigma_j^2 / \sum_{j=1}^{N}\sigma_j^2 \tag{25}$$

where Ra should be as large as possible, here the cutoff Ra=99.5%.

In this way, the snapshot matrix $\mathbf{Z}_i$ of the monitored state variable can be encoded/ decoded into a lower-dimensional score matrix $\mathbf{\Phi}$**.** Once this dimension reduction has been completed, the input-to-ranked score mapping is built as $\boldsymbol{x} \rightarrow \mathbf{\Phi}=\mathrm{F}(\boldsymbol{x})$. Like data-

driven ROM, an L-layer ANN with α outputs is used to implement the mapping between the input $\mathbf{X} \in \mathbb{R}^{n \times N}$ and the output $\mathbf{\Phi} \in \mathbb{R}^{\alpha \times N}$, as expressed by

$$\boldsymbol{z} = \mathbf{\Psi}\,\mathrm{F}(\boldsymbol{x}) \tag{26}$$

Eventually, the bi-level ROMs can be formulated in the following state-space model:

$$\begin{bmatrix} \boldsymbol{y} \\ \boldsymbol{z} \end{bmatrix} = \begin{bmatrix} \boldsymbol{B}(\boldsymbol{x}) \\ \boldsymbol{D}(\boldsymbol{x}) \end{bmatrix} = \begin{bmatrix} \mathbf{I} & 0 \\ 0 & \mathbf{\Psi} \end{bmatrix} \begin{bmatrix} \boldsymbol{G}(\boldsymbol{x}) \\ \boldsymbol{F}(\boldsymbol{x}) \end{bmatrix} \tag{27}$$

where $\mathbf{I}$ is a unit matrix.

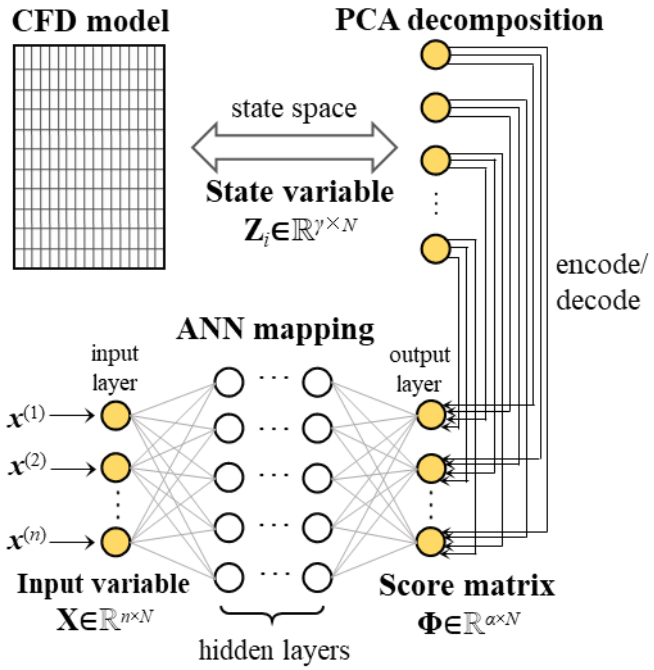

Fig. 4. The PCA-ANN approach for the construction of physics-based ROM.

3.5 Model evaluation

It is well-known that the ROM performs well at training points with ANN mapping. The true performance of a developed ROM mainly depends on how well it can predict interpolated points. In this study, 85% of the SROM samples are randomly selected as the training set to train the neural network mappings. The remaining ones included in the test set are used as interpolated points to measure the generalization error between

the outputs of the ROM and CFD model. For the data-driven ROM and physics-based ROM, the generalization errors in terms of the average relative error (avgRE) are given by

$$avgRE = \begin{cases} \dfrac{1}{N_{TE}} \sum_{j}^{N_{TE}} \left| \dfrac{y_j - y_j^{CFD}}{y_j^{CFD}} \right|, & j = 1, \ldots, N_{TE} \\ \dfrac{1}{N_{TE} \cdot \gamma} \sum_{j}^{N_{TE}} \sum_{i=1}^{\gamma} \left| \dfrac{z_{i,j} - z_{i,j}^{CFD}}{z_{i,j}^{CFD}} \right|, & i = 1, \ldots, \gamma;\ j = 1, \ldots, N_{TE} \end{cases} \tag{28}$$

where the $z_{i,j}$ and $z_{i,j}^{CFD}$ are the results of state variables at the i^{th} node of the mesh corresponding to the j^{th} sample in the test set obtained from physics-based ROM and CFD model, respectively, and N_{TE} is the sample size of the test set.

4 Stochastic optimization model

The constructed data-driven ROM that maps all input and output variables of interest can be used as a surrogate module of the CWCT system to be embedded in a sampling-based stochastic optimization model. In the optimization model, the objective is to obtain optimal solutions through the expected value maximization of the model objective distribution denoted by the exergy efficiency ratio of the CWCT system. In particular, the formulation of the objective function for maximizing the expected value of exergy efficiency ratios according to the SROM samples is given by:

$$\begin{aligned} \max \ EER^{\text{Expected}} &= \sum_{j=1}^{N} prob^{(j)} \times \left[\frac{\dot{E}x_{cw}^{in} - \dot{E}x_{cw}^{out}}{\dot{E}x_{a}^{in} + \dot{E}x_{cw}^{in} + \dot{E}x_{aux}} \right]^{(j)} \\ &= \sum_{j=1}^{N} prob^{(j)} \times f\left(\boldsymbol{x}^{(1)}, \boldsymbol{x}^{(2)} \right)^{(j)} \\ s.t. \quad & \text{Eq(1)~Eq(7)} \\ & \text{Eq(10)~Eq(19)} \\ & T_{cw}^{out} \le T_{cw}^{design} \end{aligned} \tag{29}$$

where $prob^{(j)}$ is the probability related to the occurrence of a specific SROM sample j,

T_{cw}^{design} is the design constraint that defines the upper outlet temperature of the circulating water for meeting the requirement of the cooling targets. Therefore, the final solutions are obtained by repeatedly solving the optimization model N times according to the SROM samples. After that, the physics-based ROM can be determined according to the obtained optimal input and output variables, which enables the rapid reconstruction of the thermal-, mechanical-, and chemical- exergy fluxes fields in CWCT systems.

It should be noted that only the data-driven ROM is used in the stochastic process optimization model to obtain the output stream information leaving the CWCT system, while the physics-based ROM is invoked for further exergy field investigation after the optimization is solved.

5 Case study

A small-size CWCT is presented to introduce the application of the bi-level ROMs. It is assumed the cooling tower system is located in a petrochemical park in Singapore. The original statistics of weather parameters during the years 2008~2018 are retrieved from the government database (http://www.noaa.gov), as provided in Table S-1 in SI-2. All seasons within the chosen years are taken into account. SROMPy [20] is used to generate 100 samples from the input space (N=100). The ANN used in the present case study has the following hyperparameters, L=2 and l=30. Note that, increasing the number of layers and hidden neurons has a negligible influence on the generation ability of the ANN. Besides, the CFD modelling and stochastic optimization programming are implemented via COMSOL Multiphysics 5.4 and MATLAB R2018b modelling environment, respectively. Both models are solved on a workstation with Intel four

processors Xeon E5 CPU@2.5 GHz and 32 GB RAM. In CFD modelling, the normalized residuals used for checking convergence are less than 10^{-4} for all governing equations.

In order to determine the most appropriate size of the PCs, the singular values and cumulative variance captured with varied PCs for the investigated exergy fields are presented. From Fig. 5(a), it can be found that the singular values drop sharply with the increase in PC, and the first five singular values are several orders of magnitude larger than the remaining ones. Fig. 5(b) further shows the proportion of the cumulative variance of the field data captured with the increase in the retained PCs. For this figure, the optimal number of PCs is selected as α=5, and the captured proportion of variance is close to 100%. Based on this selection, the dimensions of the field representation are all significantly reduced from 3,304 to 5, while the amounts of snapshot data stored in the thermal-, mechanical-, and chemical- exergy fields are compressed by 99.85%. To conclude, snapshot PCA shows great potential for reducing the multidimensional data set of the exergy field on the premise of maintaining good accuracy.

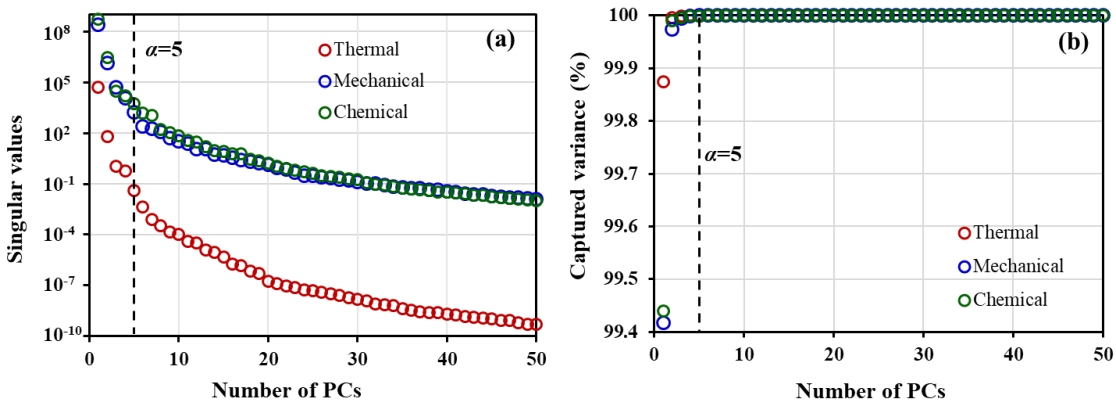

Fig. 5. (a)The singular values of the PCs and (b)the cumulative variance captured with varied PCs.

To ensure the generalization ability of the reduced models, it is necessary to investigate the statistics of relative errors of the monitored variables for the selected samples in the test set between the outputs of bi-level ROMs and CFD model. As shown in Fig. 7(a), the relative errors of the output temperature of the circulating water, as well as the output relative humidity and temperature of the air are all less than the magnitude of 1.00×10^{-3}. The corresponding avgRE for these three stream variables are 6.79×10^{-6}, 2.38×10^{-5}, and 7.29×10^{-5}. Fig. 6(b) further shows the relative errors of the monitored state variables between the physics-based ROM and the CFD model. As shown, the relative errors of the thermal-, mechanical-, and chemical- exergy fluxes are all less than the magnitude of 1.00×10^{-2}, and the corresponding avgRE are 2.41×10^{-4}, 2.86×10^{-6}, and 1.00×10^{-3}, respectively. From the statistics of these relative errors, it can be concluded that the constructed bi-level ROMs have a good generalization ability and provide sufficient confidence to perform stochastic optimization.

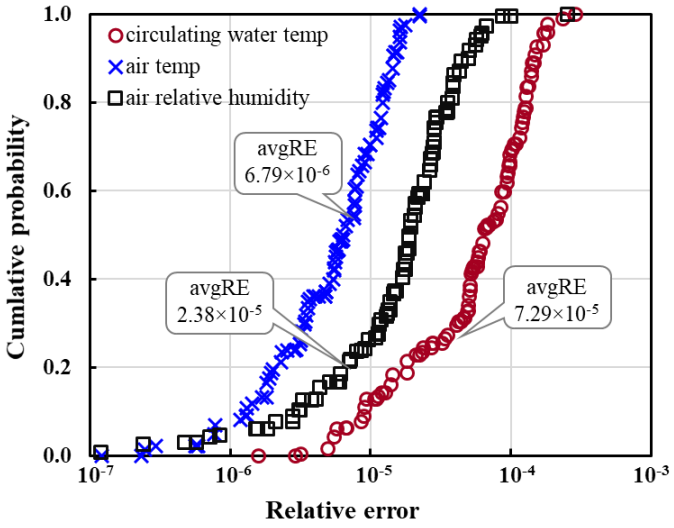

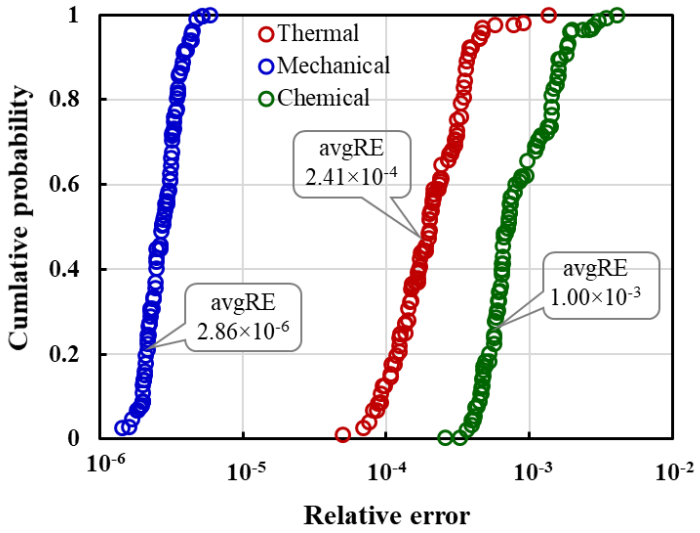

Fig. 6. Relative errors between bi-level ROMs and CFD solution. (a) data-driven ROM, (b) physics-based ROM.

The optimal solutions of the exergy efficiency ratios related to the SROM samples under distinct weather conditions are shown in Fig. 7(a). In this figure, the optimal exergy efficiency ratios denoted by green circles show a rising trend from 0.37 to 0.74 with the increase in the dry-bulb temperature of inlet air. The expected value of these optimal exergy efficiency ratios is 0.56. The corresponding probabilities of occurrence denoted by black forks have a scattered and wide distribution that ranges from 0.001 to 0.032. Fig. 7(b) further shows the optimal solutions of the air flow rate (square dots) and spray water flow rate (triangle dots) at various dry-bulb temperatures of inlet air. On the whole, the optimal values of air flow rate tend to be close to their upper limit with 6 samples having reached the upper limit. In contrast, the optimal values of the spray water flow rate are closer to their lower limit, and 12 samples have reached the lower limit. These trends indicate that, although increasing the air flow rate and decreasing the spray water flow rate contribute to the improvement of the exergy efficiency, in practice it cannot adjust them blindly due to major constraints (i.e., the

outlet temperature of spray water) used in the developed bi-level ROMs-based optimization model.

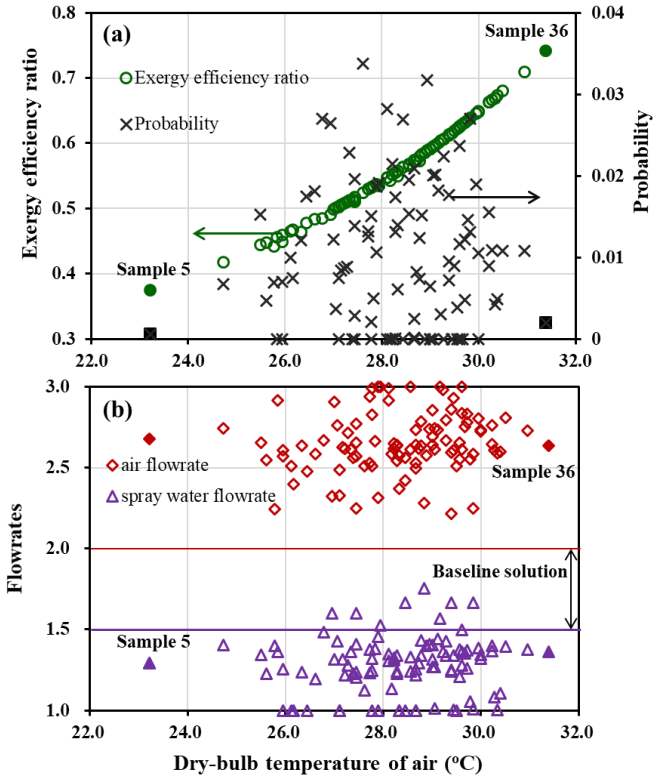

Fig. 7. Optimization results based on trained data-driven ROM. (a) exergy efficiency ratios and their probabilities and (b) control variables.

The proposed bi-level ROMs approach not only presents the optimal values of the model objective and the corresponding control variables for the CWCT system, but also reconstructs the high-fidelity fluid dynamics and reveals the complex thermal and flow fields via physics-based ROM. To better demonstrate the difference between the outputs of physics-based ROM and CFD model, two representative samples with extreme and distinct weather conditions are investigated using a baseline solution. This baseline solution directly employs a deterministic control strategy that corresponds to the expected values of the control variables listed in Table 1 (m_a=2.0 m^3/s, m_{sw}=1.5 kg/s). The two representative samples correspond to the coldest and hottest weather

conditions in the SROM samples, namely Sample 5 (T_a^{in}=23.2 ºC φ_a^{in}=0.87, *EER*=0.37) and Sample 36 (T_a^{in}=31.4 ºC, φ_a^{in}=0.57, *EER*=0.74).

According to Figs. 8 and 9, it is seen that the profiles of the three exergy fluxes predicted using physics-based ROM are comparable to those from CFD simulation, and the distortions of the images in some local areas are hardly observed. Comparing these profiles, it may be concluded that the outputs of physics-based ROM maintain high accuracy and no observable difference at the interpolated points. Besides, it should be highlighted that the bi-level ROMs approach is capable of significantly reducing the computational time and resources as compared to the use of principled CFD models; i.e., the total time for reconstructing the exergy profiles inside of the CWCT system from rigorous CFD simulations requires approximately 3 days, while the developed approach only takes 20~30 s for the same case.

For the investigated samples, as the inlet air flows upward and contacts with falling spray water, it is gradually saturated with the spray water and heated by the circulating water inside the coil tubes. This decreases the chemical- exergy flux and increases the thermal exergy flux in the direction of the bottom to top in CWCT system, as shown in Figs. 8 and 9. Through further comparing the field profiles between Sample 5 and Sample 36, the distributions of thermal- and chemical- exergy fluxes have obvious variations in different weather conditions. For example, in comparison with Sample 36, Sample 5 has a greater temperature difference between the circulating water and inlet air, which results in a more obvious change of the thermal exergy distributed in the fluid field. Unlike chemical- and thermal exergy fluxes, it is interesting that the optimal

values of mechanical exergy flux for both Sample 5 and Sample 36 are negative since the applied pressure in the CWCT system is smaller than that of the reference pressure in the dead state. Besides, they have almost the same contours that range from -1.2×10^3 ~0 W/m^2, indicating that the weather conditions have a negligible influence on the distribution of the mechanical exergy flux.

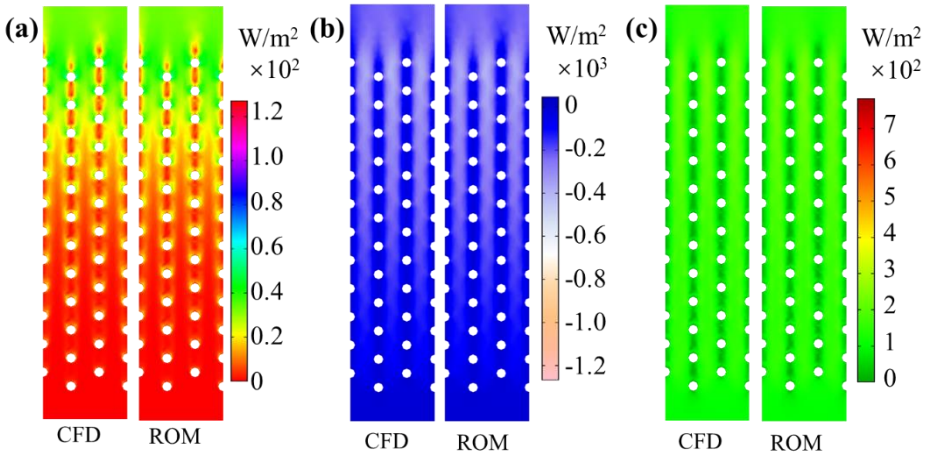

Fig. 8. The profiles of (a) thermal-, (b) mechanical-, and (c) chemical- exergy fluxes in the case of Sample 5 obtained from CFD solution and physics-based ROM.

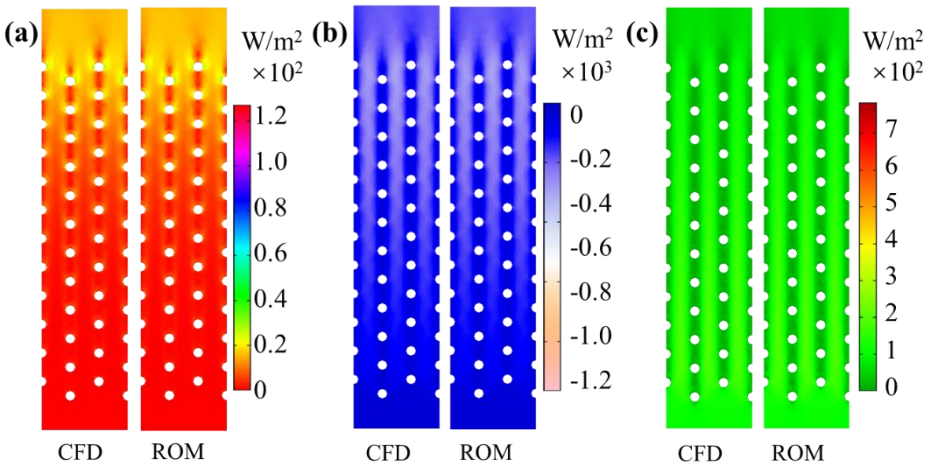

Fig. 9. The profiles of (a) thermal-, (b) mechanical-, and (c) chemical- exergy fluxes in the case of Sample 36 obtained from CFD solution and physics-based ROM.

To further reveal the influence of the optimal solution on the heat and mass transfer

processes, the three exergy fields (see Figs. 8 and 9) obtained from the baseline solution are compared with those obtained from the optimal solution (see Section 4). Figs. 10~12 illustrate the exergy flux profiles in the CWCT system obtained from the optimal and baseline solutions.

As shown in Fig. 10, by and large, the two solutions yield similar thermal exergy flux profiles for both two samples. The amplified areas of the selected top tubes further show that the values of the contours of the thermal exergy fluxes are in the ranges of 3.0~55.1 W/m^2 (Sample 5) and 1.3~34.4 W/m^2 (Sample 36) for the baseline solution, 8.7~ 94.7 W/m^2 (Sample 5) and 1.8~45.1 W/m^2 (Sample 36) for the optimal solution. As for the mechanical exergy flux shown in Fig. 11, the longitudinal variations of the fluid field appear more evident between the two solutions for both two samples. Taking Sample 5 as an example, the mechanical exergy fluxes have about 3 times increase from -323.0~-36.5 W/m^2 for the baseline solution to -774.5~-117.6 W/m^2 for the optimal solution. Similar to the mechanical exergy flux, the chemical exergy flux obtained from the optimal solution is much higher than that of the baseline solution. As shown in Fig. 12, the values of contours of the chemical exergy fluxes of Sample 5 remarkably increase from 41.7~119.1 for the baseline solution to 113.8~ 651.4 W/m^2 for the optimal solution. In the case of Sample 36, they correspondingly have increased by 3 times from 18.3~56.4 W/m^2 to 55.0~163.2. These increases in mechanical- and chemical exergy fluxes are mainly because the optimal solution can effectively strengthen the heat and mass transfer processes inside of the CWCT system in extreme weather conditions by using a higher air flow rate (m_a=2.68 m^3/s for the Sample 5 and 2.63 m^3/s for the Sample

36) and a lower spray water flow rate (m_{sw} =1.29 kg/s for the Sample 5 and 1.36 kg/s for the Sample 36). This highlights the importance of considering the uncertainty on weather parameters in the optimal operation of the cooling water system.

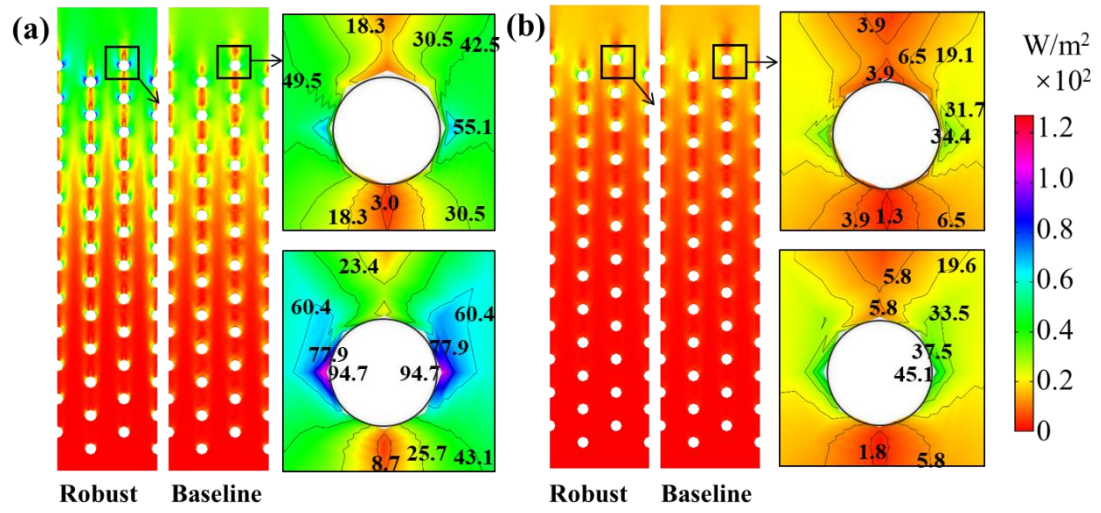

Fig. 10. Comparison of the thermal exergy fields in the CWCT system. (a)Sample 5; (b) Sample 36.

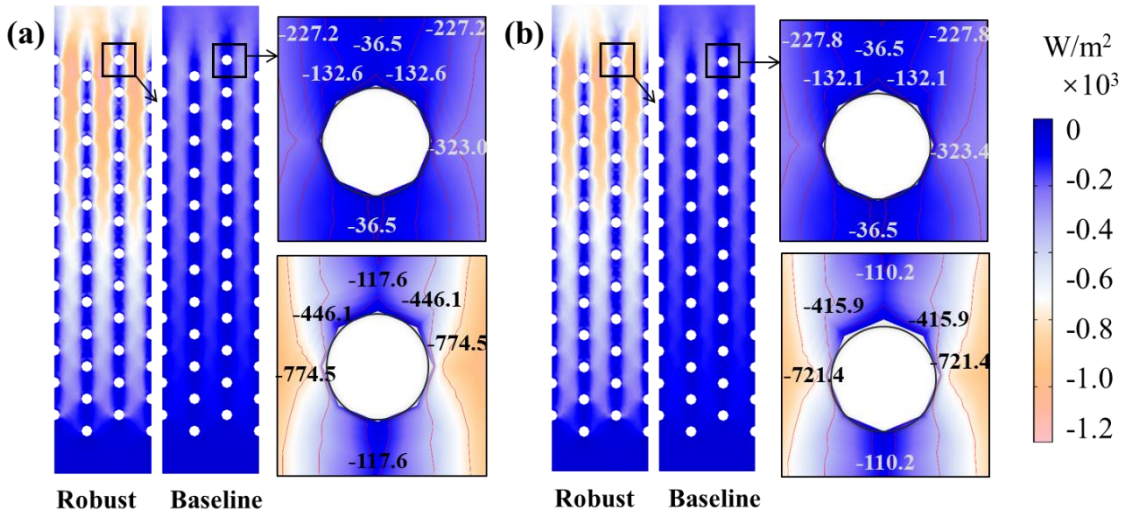

Fig. 11. Comparison of the mechanical exergy fields in the CWCT system. (a)Sample 5; (b) Sample 36.

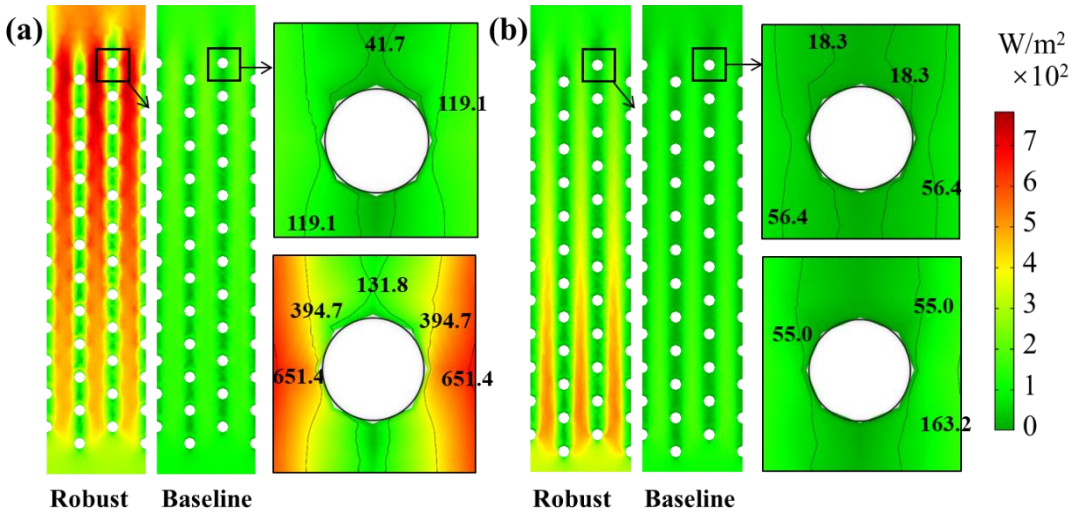

Fig. 12. Comparison of the chemical exergy fields in the CWCT system. (a)Sample 5; (b) Sample 36.

In summary, the reusltes of the case study illustrates the main strengths of the proposed bi-level ROMs approach—the ability to yield optimal exergy efficiency ratios and exergy field profiles of the CWCT systems in a computationally efficient manner. The computational time is significantly reduced from several days or more for batch CFD simulations to only a few seconds for the proposed approach, which makes the tasks of real-time prediction and online analysis realizable. The stochastic optimization improves the robustness of the CWCT system considering environment variations. Finally, the analysis of the exergy field allows researchers to gain insights into the distributed exergy parameters in the cooling tower.

6 Conclusion

This work focused on the physical inspection of the spatially distributed exergy parameters inside of the cooling tower systems. It proposed a bi-level ROMs approach that comprises data-driven ROM and physics-based ROM for minimizing the expected value of the exergy efficiency ratios and obtaining the optimal exergy fields in the

CWCT system with consideration of weather variations. Four statistical steps, namely DoE, multi-sample CFD simulations, model reduction, and model evaluation were used in the development of the bi-level ROMs. In particular, the uncertainty associated with input variables was propagated via multi-sample CFD simulations of the CWCT model for each of the samples. The results of the state and output variables stored in the CFD solutions were used to construct the physics-based and data-driven models by combining PCA and ANN methods. The developed ROMs were embedded within the sampling-based stochastic optimization model for minimizing the expected value of the exergy efficiency ratios and obtaining the optimal exergy fluxes fields inside of the CWCT system.

The applicability of the proposed approach was illustrated through a small size CWCT. The result of the case study showed that the optimal exergy efficiency ratios ranged from 0.37 to 0.74 with the rise of the dry-bulb temperature of inlet air, and the expected value of the exergy efficiency ratio was 0.56. The exergy field investigation indicated that both mechanical- and chemical exergy fluxes obtained from the optimal solution were about 3 times higher than that of the baseline solution, which highlighted the importance of considering the environmental variations in the optimal operation of the cooling water system.

Although the case study showed that the proposed bi-level ROMs approach was effective and efficient for the presented study, many issues still need to be dealt with in future work, e.g., how to further reduce the sizes of the sampled points, the neurons in the hidden layer, and the retained PCs, etc. Besides, the proposed approach can also be

applied for handling the geometric design of heat transfer equipment with complex structures through the use of experimental design and analytic hierarchical process. Finally, depth analysis of convergence properties and process constraints for the stochastic optimization model would enhance the capability to converge to local or global optima.

Acknowledgments

Financial supports from the National Natural Science Foundation of China (No. 51776228), the Chinese Universities Scientific Fund (No. 20lgpy01) are gratefully acknowledged.

References

[1] Zhu Q, Zhang B, Chen Q, et al. Model Reductions for Multiscale Stochastic Optimization of Cooling Water System Equipped with Closed Wet Cooling Towers, Chemical Engineering Science, 2020: 115773.

[2] Zhang L, Liu X, Jiang Y. Exergy analysis of parameter unmatched characteristic in coupled heat and mass transfer between humid air and water, International Journal of Heat and Mass Transfer, 2015, 84: 327-338.

[3] Qu J H, Liu H, Pan M, et al. Optimisation and Analysis Based on Bi-Level Reduced-Order Model for Coupled Heat and Mass Transfer Processes Under Uncertainty, Chemical Engineering Transactions, 2020, 81: 727-732.

[4] Ghazani M A, Hashem-ol-Hosseini A, Emami M D. A comprehensive analysis of a laboratory scale counter flow wet cooling tower using the first and the second laws of thermodynamics, Applied Thermal Engineering, 2017, 125: 1389-1401.

[5] Zhang L, Song X, Zhang X. Theoretical analysis of exergy destruction and exergy flow in direct contact process between humid air and water/liquid desiccant solution, Energy, 2019, 187: 115976.

[6] Singh K, Das R. Improved quantification of exergy destruction in mechanical cooling tower considering all tower inlet parameters, Journal of Heat Transfer, 2018, 140(5).

[7] Singh K, Das R. Exergy optimization of cooling tower for HGSHP and HVAC applications, Energy Conversion and Management, 2017, 136: 418-430.

[8] Xie X, Liu H, He C, et al. Deciphering the heat and mass transfer behaviors of

staggered tube bundles in a closed wet cooling tower using a 3-D VOF model, Applied Thermal Engineering, 2019, 161: 114202.

[9] Barrasso D, Tamrakar A, Ramachandran R. A reduced order PBM–ANN model of a multi-scale PBM–DEM description of a wet granulation process, Chemical Engineering Science, 2014, 119: 319-329.

[10] Boukouvala F, Gao Y, Muzzio F, et al. Reduced-order discrete element method modeling, Chemical Engineering Science, 2013, 95: 12-26.

[11] Yu M, Miller D C, Biegler L T. Dynamic reduced order models for simulating bubbling fluidized bed adsorbers, Industrial & Engineering Chemistry Research, 2015, 54(27): 6959-6974.

[12] Aversano G, Bellemans A, Li Z, et al. Application of reduced-order models based on PCA & Kriging for the development of digital twins of reacting flow applications, Computers & Chemical Engineering, 2019, 121: 422-441.

[13] Bellemans A, Aversano G, Coussement A, et al. Feature extraction and reduced-order modelling of nitrogen plasma models using principal component analysis, Computers & Chemical Engineering, 2018, 115: 504-514.

[14] Cheng Y, Zheng W, Sung-Kwun O, et al. Ensemble fuzzy radial basis function neural networks architecture driven with the aid of multi-optimization through clustering techniques and polynomial-based learning, Fuzzy Sets and Systems, 2021, In press.

[15] Deng C, Zheng H, Fu M, et al. An efficient method of approximate particular solutions using polynomial basis functions, Engineering Analysis with Boundary

Elements, 2019, 111: 1-8.

[16] Atkinson S, Zabaras N. Structured Bayesian Gaussian process latent variable model: Applications to data-driven dimensionality reduction and high-dimensional inversion, Journal of Computational Physics, 2019, 383: 166-195.

[17] Najm H N. Uncertainty quantification and polynomial chaos techniques in computational fluid dynamics, Annual Review of Fluid Mechanics, 2009, 41: 35-52.

[18] Wuyan L, Yongcai L, Wenxing S, et al. Energy and exergy study on indirect evaporative cooler used in exhaust air heat recovery, Energy, 2021, 235, 121319.

[19] Lang Y, Malacina A, Biegler L T, et al. Reduced order model based on principal component analysis for process simulation and optimization, Energy & Fuels, 2009, 23(3): 1695-1706.

[20] Warner, J. E. (2018). Stochastic reduced order models with Python (SROMPy). NASA/TM-2018-219824.

[21] Sarkar S, Warner J E, Aquino W, et al. Stochastic reduced order models for uncertainty quantification of intergranular corrosion rates[J]. Corrosion Science, 2014, 80: 257-268.

[22] Qiming Q, Hua L, Chang H, et al. Sustainable retrofit of petrochemical energy systems under multiple uncertainties using the stochastic optimization method, Computers & Chemical Engineering, 2021, 151, 107374.